CrystEngComm

Accepted Manuscript

ROYAL SOCIETY OF CHEMISTRY

www.rsc.org/crystengcomm

Journal Name

RSCPublishing

ARTICLE

Tailoring of {116} faceted single crystalline anatase nanosheets array and improved electrochemical performance

Cite this: DOI: 10.1039/x0xx00000x

Feng Li,[a] Xiaoning Li,[a] Shangfeng Yang,[ac] Zhengping Fu,*[abc] and Yalin Lu*[abc]

Received 00th January 2012,
Accepted 00th January 2012

DOI: 10.1039/x0xx00000x

www.rsc.org/

{116} faceted single crystalline anatase nanosheets array could exhibit excellent electrochemical and photocatalytic performance. In order to optimize the performance, structures of the nanosheets arrays were studied by changing the growth parameters, including growth temperature, initial reactant concentration, precursors and additives, etc. The nanosheets array grown under high temperature and with an additional surfactant CTAB possesses highly preferred {116} orientation, and shows the upright diamond structure. The sample exhibits higher reduction capacity and electrochemical reversibility. In the growth of {116} faceted anatase nanosheets array, hydrofluoric acid was also uncovered to act as the hydrolysis inhibitor, rather than as the capping agent. Extra hydrofluoric acid will suppress the degree of the preferred orientation.

1. Introduction

Synthesis of TiO_2 nanostructured arrays with specific morphology and orientation has attracted much attention due to their potential applications in electrocatalysis, sensors, hydrogen production, lithium batteries, and dye-sensitized solar cells.[1-5] Up to now, most of such arrays were composed of polycrystalline TiO_2 nanowires or nanotubes, the performances of which might be limited because of the scattering and trapping of electron at grain boundaries.[6] On the other hand, single crystalline TiO_2 nanosheets can offer large percentage of specific facets than nanowires and nanotubes, which was favoured by diverse applications.[5] Inspired by the work of Yang, extensive efforts have been devoted to synthesize various types of anatase TiO_2 nanosheets exposed with reactive facets such as {001} and {100}.[7-10] However, there were few works on TiO_2 nanosheet exposed with high indexed facets, though they have shown excellent properties in many applications.

In our previous work, we have synthesized {116} faceted single crystalline nanosheets array on FTO substrate.[11] Compared with low-index facets, {116} facets possess more low-coordinated Ti atoms and higher surface energy (ESI, Fig. S1†),[11] therefore, they are expected to be more reactive and attractive for various potential applications. Commonly, properties of such nanomaterials are closely related to structural parameters such as morphology, density, orientation, sheet size, aspect ratio, et al, and the structural parameters can be further controlled by the deposition details.[12] By carefully tuning the titanium / oleic acid / oleylamine ratio, Dinh et al successfully prepared anatase TiO_2 with a variety of shapes.[13] Gordon et al had shown that the morphology of TiO_2 nanocrystals could be sensitively manipulated by the choice of titanium precursors, which exhibited different photocatalytic activities in the production of hydrogen.[14] Therefore, in order to optimize the electrochemical properties via structure tailoring, which will be important for lithium batteries and electrocatalysis applications, systematic works are required to clarify the effects of growth parameters on the nanosheets array structure.

In this work, we focused on a systematic investigation of the growth parameters' effects on the morphology of {116} facets dominated nanosheets array. Function of hydrofluoric acid for the growth of {116} faceted nanosheets array was illustrated. Comparing with previous work, higher reduction capacity and electrochemical reversibility were obtained in the upright diamond structured sample with highly preferred orientation, which was synthesized under high temperature and with an additional surfactant (CTAB).

2. Experimental

2.1. Synthesis of TiO_2 nanosheets array

In a typical synthesis, the FTO coated glass was ultrasonically cleaned sequentially in acetone, ethanol, distilled water for 15 min each, subsequently immersed in 1 M NaOH aqueous solution for 24 h, then rinsed with distilled water, and finally dried in the air. A TiO_2 seed layer was prepared on the

as-cleaned FTO coated glass by spin coating method. Separately, 0.5-2.0 ml of titanium butoxide was added dropwise to 15 ml of ethanol. The mixture was stirred at ambient conditions for 5 min before the addition of 0.5-2.0 ml of hydrofluoric acid. After stirring for another 5 min, the mixture was transferred to a dried 50 ml Teflon-lined autoclave, and a piece of FTO glass coated with TiO_2 seed was placed vertically in the autoclave, and then the autoclave was kept at 140-200 ºC for 12 h. After cooling down to room temperature, the FTO substrate was taken out, and then ultrasonically cleaned with ethanol and distilled water for several times, followed by drying at 65 ºC in an oven. Effects of titanium precursors and additional surfactants such as ethylenediamine (EDA), ethylenediaminetetraacetic acid (EDTA), oleic acid (OA), cetyltrimethylammonium bromide (CTAB), sodium fluoride (NaF), and polyvinylpyrrolidone (PVP) were also studied.

2.2. Characterization and measurements

X-ray diffraction patterns were obtained by using a TTR-III X-ray diffractometer with Cu Kα radiation (λ=1.5418Å). The morphologies of samples were examined by FESEM (JSM-6700F) and TEM (JEM-2011). The electrochemical performances of the nanosheets arrays were measured in a three-electrode electrochemical cell with the scan rate of 50 mVs^{-1} on an electrochemical workstation (CHI660E, Shanghai Chenhua Device Company, China). The nanosheets array sample, a Pt wire, and an Ag/AgCl electrode (saturated KCl) were used as the working electrode, the counter electrode, and the reference electrode respectively, while a solution of 0.5 M H_2SO_4 was taken as the electrolyte.

3. Results and discussion

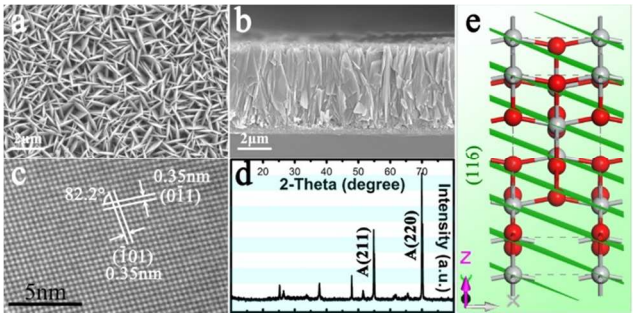

Fig. 1 (a, b) Typical FESEM images of nanosheets array grown on FTO substrate in 15 ml ethanol, 1.0 ml titanium butoxide, and 1.0 ml hydrofluoric acid at 200 °C for 12 h. (c) HRTEM image of nanosheet. (d) XRD pattern of nanosheets array. (e) Crystal structure diagram viewed from [06$\bar{1}$] axis.

As shown in Fig. 1a and b, the fishnet-structured film covers uniformly on the FTO substrate and assembled by nanosheets with 4.71 μm in side length and 30-35 nm in thickness. The nanosheets stand perpendicularly on the FTO substrate and cross into each other to avoid aggregation and collapsing. Fig. 1c shows HRTEM image of a typical nanosheet. The spacings between lattice fringes are 0.35 nm, which can be attributed to the {101} planes of anatase TiO_2. The interfringe angle is 82.2°, further indicating <111> axis as the diffraction axis, and identifying {116} facets as the surface of the nanosheets. The SAED pattern is also consistent with the simulated electron diffraction pattern for single crystalline along <111> axis (ESI, Fig. S2†). XRD pattern in Fig. 1d reveals that the crystal structure of the array structure is anatase TiO_2 (JCPDF no. 89-4921, a=b=0.3777 nm, c=0.9501 nm). Due to that the {116} facets exposed nanosheets stand perpendicularly on the FTO substrate, the diffraction peaks of (220) and (211) planes, which are perpendicularly to the equivalent facets of {116} facets, are significantly enhanced (ESI, Fig. S2†). Furthermore, the strongest diffraction peak of (220) plane suggests that the vertical growth direction can be indexed as <1 $\bar{1}$ 0> zone, perpendicular to the {1$\bar{1}$0} facets. Crystal structure in Fig. 1e is anatase TiO_2 viewed from [06$\bar{1}$] axis, while the (116) facets marked with green rhomboid stand vertically and perpendicular to [111] axis.

3.1. Effect of Growth Temperature

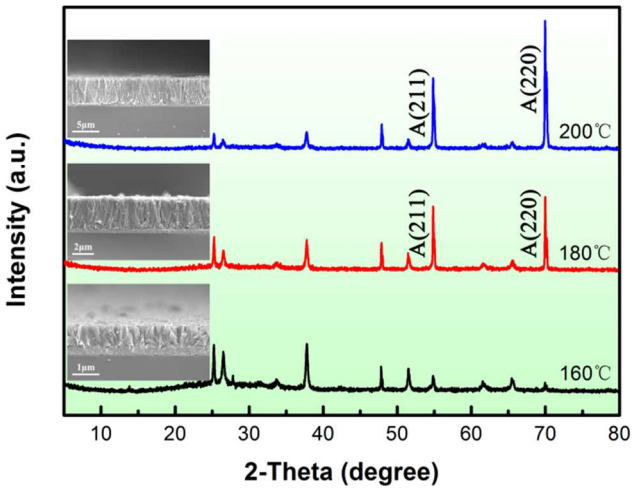

Fig. 2 XRD patterns of nanosheets array grown on FTO substrate in 15 ml ethanol, 1.0 ml titanium butoxide, and 1.0 ml hydrofluoric acid at 160, 180, and 200 °C for 12 h. The insets are corresponding cross-sectional FESEM images.

The lowest temperature to grow nanosheets array on the FTO substrate is 160 ºC, and nothing was obtained on the substrate when the temperature was lower. The growth rate of nanosheets array can be deduced from the thickness of the array film. FESEM images in Fig. 2 indicate that the growth rates at 200 ºC and 180 ºC are 6 and 3.7 times of that at 160 ºC, consist well with the peak intensities of (211) and (220) planes. Comparing with the growth rate at 180 ºC, the increasing growth rate slows down at 200 ºC, which can be attributed to the exhaustion of the precursor. On the other hand, the relative peak intensities of (211) and (220) planes are significantly increased for the sample grown at 180 ºC and 200 ºC, revealing that higher temperatures are more favoured by preferred orientation.

3.2. Effect of Initial Reactant Concentration

As shown in Fig. S3 (ESI, †), there are three different growth stages during the increasing of the initial reactant concentration. The side length of the nanosheets increased from 2.55 μm to

4.76 μm, while the thickness increased slightly by increasing the reactant volume from 0.5 ml to 1.0 ml (Stage S3a-S3c). However, the side length of the nanosheets was almost the same, while the thickness was multiple in spite of increasing the reactant volume from 1.0 ml to 1.5 ml (Stage S3c-S3e). Nanosheets grown with the reactant volume of 1.5 ml (ESI, Fig. S3e†) had a layer structure, revealing that the increased reactant concentration promoted repeated secondary nucleation and growth on the surface of the nanosheets. On stage S3e-S3g, both the side length and thickness of the nanosheets decreased rapidly when increasing the reactant volume from 1.5 ml to 2.0 ml. Meanwhile, the nanosheets stood obliquely to the substrate, which can be attributed to that the nucleation and vertical growth of the nanosheets were strongly inhibited by high concentration of HF.

3.3. Effect of Hydrofluoric Acid

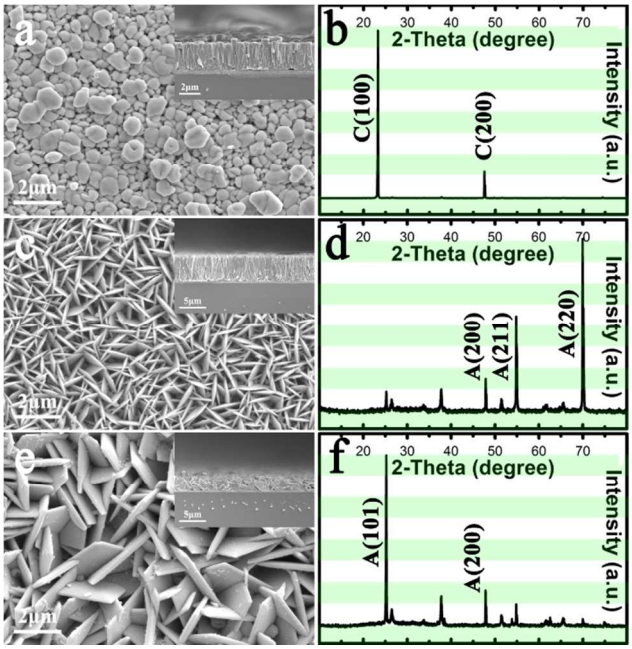

Fig. 3 FESEM images and the corresponding XRD patterns of nanosheets arrays grown on FTO substrate at 200 ºC for 12 h with 15 ml ethanol, 1.0 ml titanium butoxide and different amounts of hydrofluoric acid: (a,b) 0.5 ml, (c,d) 1.0 ml, (e,f) 1.5ml.

No TiO_2 nanosheet was obtained on the FTO substrate if the hydrofluoric acid was replaced by deionized water, however, white precipitation was found at the bottom of the vessel, revealing that the hydrofluoric acid acted not only as a precursor but also a hydrolysis inhibitor. As shown in Fig. 3a, cubic phase $TiOF_2$ nanorods were obtained (JCPDF no. 77-0312, a=b=c=0.3798 nm) when the amount of hydrofluoric acid was 0.5 ml. The products turned into anatase TiO_2 nanosheets by doubling the volume of hydrofluoric acid to 1.0 ml. As the amount of hydrofluoric acid was increased to 1.5 ml, the density of the anatase TiO_2 nanosheets decreased, resulting in the leaning of the nanosheets to the substrate and the increase of (101) diffraction peak, which can be attributed to the inhibited nucleation on the substrate and the erosion effect of hydrofluoric acid.

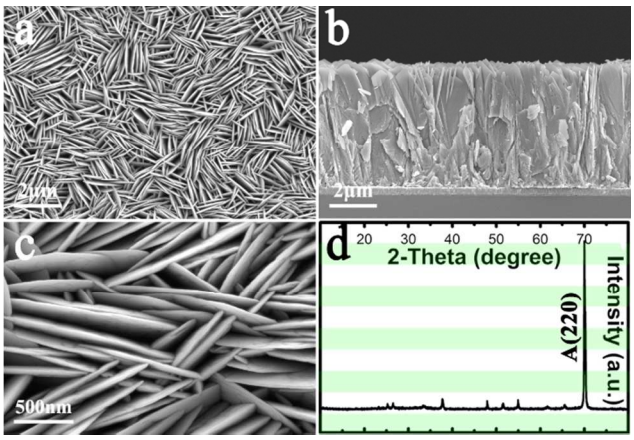

Fig. 4 (a, b, c) FESEM images of nanosheets array grown on FTO substrate at 200 ºC for 12 h in 15 ml ethanol, 1.0 ml titanium butoxide, 0.5 ml hydrofluoric acid, and additional 0.5 ml deionized water. (d) Corresponding XRD pattern.

Typically, $TiOF_2$ could be obtained with high relative concentration of HF in the growth solution. However, in present work, cubic $TiOF_2$ nanorods were grown with low relative concentration of HF, while anatase TiO_2 nanosheets were gotten with higher relative concentration of HF (Fig. 3c and 3e). To investigate the mechanism for the formation of $TiOF_2$, extra 0.5 ml deionized water was added into the growth solution together with 0.5 ml hydrofluoric acid. The products were turned from cubic $TiOF_2$ nanorods to anatase TiO_2 nanosheets with highly preferred orientation (Fig. 4). This result revealed that in the solution with low H_2O concentration, HF will took place of H_2O to hydrolyze titanium butoxide, as a result, part of the oxygen in TiO_2 was replaced by fluorine, and then $TiOF_2$ nanorods were obtained.

The side lengths of TiO_2 nanosheets in Fig. 3c, Fig. 3e and Fig. 4a are 4.71 μm, 2.73 μm and 5.32 μm, while the thicknesses are 35 nm, 100 nm and 25 nm, respectively. Comparing TiO_2 nanosheets in Fig. 3c and Fig. 3e, the extra 0.5 ml hydrofluoric acid led not only to the decreased side length but also the increased thickness, revealing that the nucleation on the seed layer and the growth on the vertical direction were significantly inhibited, while the growth along the normal direction of the nanosheets surface was less limited. In other words, the result suggests that the ethanol and F^- ion preferred to adsorb on different facets. Furthermore, comparing TiO_2 nanosheets in Fig. 3c and Fig. 4a, the replacement of 0.5 ml hydrofluoric acid with deionized water resulted in the increased side length and the decreased thickness, suggesting that the growth on the vertical direction was limited by the hydrofluoric acid, while the growth along the normal direction of the nanosheets surface was not. Meanwhile, different to the XRD pattern of the sample grown with 1.0 ml hydrofluoric acid (Fig. 3d), the diffraction peak of (220) plane in the sample grown with 0.5 ml hydrofluoric acid and 0.5 ml deionized water was significantly enhanced (Fig. 4b), while the other diffraction peaks almost disappeared, indicating that TiO_2 nanosheets

grown with 0.5 ml hydrofluoric acid and 0.5 ml deionized water exhibited much better orientation and further confirmed <1$\bar{1}$0> zone as the vertical growth direction. Based on the above SEM and XRD results, we can conclude that HF acts as hydrolysis inhibitor more than capping agent in this system and extra HF will decrease the orientation.

3.4. Effect of Titanium Precursor

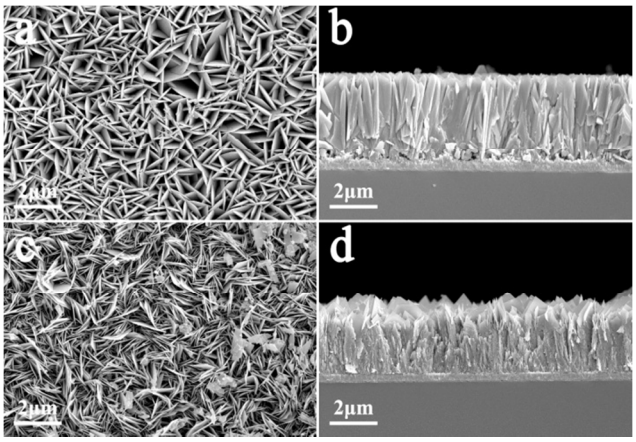

Fig. 5 FESEM images of nanosheets array grown on FTO substrate at 200 ºC for 12 h in 15 ml ethanol and 1.0 ml hydrofluoric acid with different titanium precursors. (a, b) 1.0 ml titanium isopropylate, (c, d) 1.0 ml titanium tetrachloride.

Titanium isopropylate and titanium tetrachloride were also adopted to substitute titanium butoxide to grow nanosheets array on FTO substrate. The nanosheets array synthesized with titanium isopropylate possessed a similar morphology and XRD pattern to that synthesized with titanium butoxide (Fig. 5a and b, ESI, Fig. S4†). When titanium tetrachloride was used, the nanosheets turned into angular rhombus with a thickness of 10-15 nm (ESI, Fig. S5†). The angular rhombus can be attributed to the occupation of Cl^- on the {101} facet, while the reduction of the side length and thickness possibly due to the more effective inhibition of hydrochloric acid for the nucleation on the surface of nanosheets, which generated in the hydrolysis process of titanium tetrachloride. On the other hand, hydrochloric acid will inhibit the ionization of HF, and weaken the influence of HF on TiO_2 nanosheets, which may increase the thickness of the nanosheets.

3.5. Effect of Adding Surfactant or Salts

For the synthesis of {001} facets exposed TiO_2 nanosheets, OA and fluoride have been playing important roles on the morphology during the facets engineering process.[14] However, the addition of OA and NaF had little effect on the morphology of {116} facets exposed TiO_2 nanosheets, indicating the distinct engineering mechanism (ESI, Fig. S6†). Nothing was grown on the FTO substrate with the addition of EDA, EDTA, and PVP. When the surfactant was switched to CTAB, the morphology changed greatly. As shown in Fig. 6a and Fig. 6b, the morphology of TiO_2 looked like 'nanorods' in the vertical view. However, the cross view in Fig. 6c revealed that the 'nanorods' turned out to be rhombus nanosheets stood on the substrate perpendicularly with one angle, which was sketched in Fig. 6d. Compared with the (211) peak in Fig. S7 (ESI, †), (220) peak was significantly enhanced, exhibiting the same orientation with the others, which can be attributed to that the more uniform orientation and morphology of the nanosheets. The peculiar morphology possibly due to CTAB occupied on the specific facets of the nanosheets ({101} facets) and the growth of specific facets was inhibited, or CTAB induced recrystallization of the specific facets of the nanosheets. More details will be investigated in our future work.

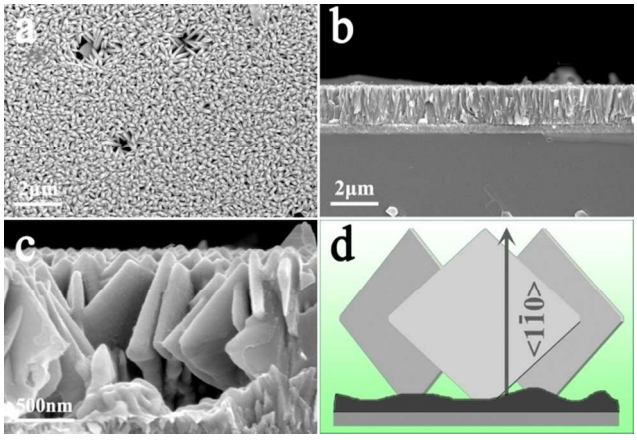

Fig. 6 (a, b, c) FESEM images of nanosheets array grown on FTO substrate in 15 ml ethanol, 1.0 ml titanium butoxide, and 1.0 ml hydrofluoric acid with 0.5 g CTAB at 200 ºC for 12h. (d) Scheme of the corresponding arrangement of nanosheets.

3.6. Growth Mechanism

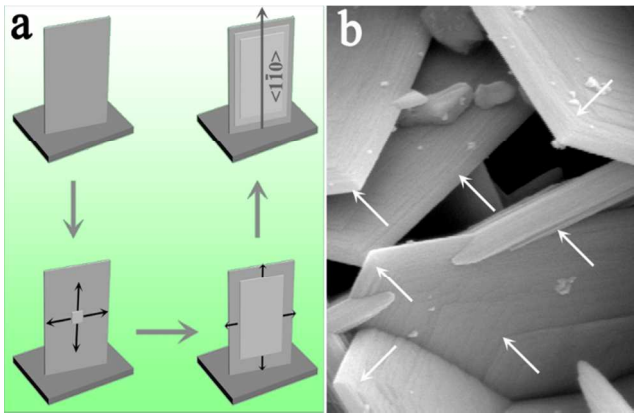

Scheme 1 (a) Schematic drawing of the growth mechanism. (b) Corresponding growth traces of the nanosheets.

Based on the above experimental results, the possible growth mechanism is proposed and illustrated as Scheme 1. In this alcohol-thermal system, ethanol acts as the solvent, while titanium butoxide is used as the titanium precursor. Hydrofluoric acid acts as a hydrolysis inhibitor by ensuring an acid condition. A small amount of water from the hydrofluoric acid solution serves as the water source. With the rise of temperature, water may diffuse from the solution and aggregate

on the hydrophilic TiO_2 seed layer coated FTO substrate surface. Simultaneously, titanium precursor will hydrolyze with water at the interface of water/TiO_2 seed layer, leading to the nucleation and growth on the substrate. In previously reported works, hydrofluoric acid was used as capping agent to engineer {001} facets, minimizing the surface energy of {001} facets, while hydrofluoric acid played a negative role in keeping the highly preferred orientation in this work, suggesting that ethanol acted as the preferred capping agent instead. Ethanol was believed to play a significant role in the modification of TiO_2 structure and properties.[15] Due to the minimization of the surface energy, ethanol will absorb preferentially on the {116} facets, limiting the growth along directions vertical to {116} facets. The growth of nuclei along directions parallel to the {116} facets turns to be faster than that along <111> directions, and then nanosheets will be formed as a result. As a return, the {116} facets of the nanosheets provide more additional nucleation sites, another round of nucleation and growth will proceed on the surface of nanosheets. The growth mechanism is further confirmed by the growth terraces indicated by the SEM images shown in Scheme 1b and indicated by white arrows. On the other hand, the initially formed hexagonal $TiOF_2$ may also play a significant role in the growth process, which may provide a lattice structure substrate with preferred orientation for the growth of anatase TiO_2 nanosheets with highly preferred orientation.

3.7. Electrochemical performance

Electrochemical performance of the nanosheets array synthesized via different conditions with different degrees of preferred orientation were evaluated by the cyclic voltammetry and shown in Fig. 7, as well as in Table 1. For convenience, the nanosheets array shown in Fig. 6a, Fig. 3e and Fig. 4a are named as NF-a, NF-b and NF-c respectively. The anodic peaks in the cyclic voltammograms can be attributed to $Ti^{4+} + e^- \rightarrow Ti^{3+}$. Comparing with NF-b, NF-c and NF-116 in our previous work, NF-a exhibits the smallest cathodic peak potential, leading to the best reduction capacity. Meanwhile, all separation between the peak potentials are small, while NF-a exhibits the highest electrochemical reversibility with the smallest separation of 68 mV.[16] Furthermore, compared with NF-001 and P25 in our previous work, NF-a, NF-b and NF-c all exhibit better reduction capacity and significantly enhanced electrochemical reversibility. Therefore the electrochemical performance was optimized by tailoring the growth parameters. The enhanced electrochemical performance of {116} facets exposed nanosheets array electrode can be attributed to the more favorable atomic structure, which possess much more three, five-coordinated Ti atoms, providing more active reaction sites for the electrochemical reactions,[17] and narrowing the band gap of the surface layer.[18] Meanwhile, optimized preferred orientation and structure will enhanced the electrochemical performance further. Based on the enhanced electrochemical performance, {116} facets exposed nanosheets array presents promising applications in the photoelectrochemical field.

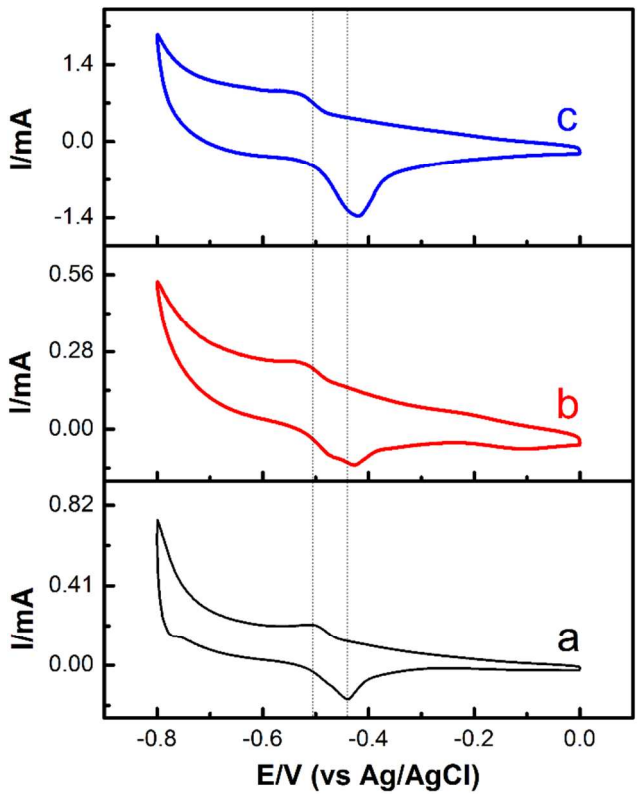

Fig. 7 Cyclic voltammograms of nanosheets array grown on FTO substrate at 200 ºC for 12 h in 15 ml ethanol, 1.0 ml titanium butoxide with (a) 1.0 ml hydrofluoric acid and 0.5 g CTAB, (b) 1.5 ml hydrofluoric acid, (c) 0.5 ml hydrofluoric acid and 0.5 ml H_2O in 0.5 M H_2SO_4. Scan rate: 50 mVs^{-1}.

Table 1. Electrochemical characteristics of nanosheets array.

	Epa[a]/V	Epc[b]/V	Ep[c]/V	(ipa[d]/ipc[e])[f]
NF-a	-0.438	-0.506	0.068	1.5
NF-b	-0.428	-0.538	0.11	2.205
NF-c	-0.42	-0.544	0.124	2.879
NF-116pre	-0.385	-0.515	0.13	1.046
NF-001	-0.305	-0.605	0.3	2.015
P25	-0.275	-0.615	0.34	2.757

[a] Anodic peak potential. [b] Cathodic peak potential. [c] Peak separation potential. [d] Anodic peak current. [e] Cathodic peak current. [f] Ratio for anodic and cathodic peak currents.

4. Conclusions

In summary, the growth of {116} faceted single crystalline anatase nanosheets array was investigated systematically and the possible growth mechanism was also proposed. Nanosheets arrays with various structures were obtained by the tailoring the growth parameters. By usage of additional surfactant CTAB, sample with the best electrochemical performance was obtained. During the synthesis, HF acted as the hydrolysis inhibitor more than capping agent in this system, and extra HF would suppress the degree of preferred orientation. Other high-index facets exposed nanosheets may be synthesized by the similar strategy, leading to better understanding of the

photoelectrochemical process on these facets and improved performance in the corresponding field.

Acknowledgements

This work was supported by the National Basic Research Program of China (2012CB9222000) and Provincial Natural Science Research Project of Anhui Colleges (KJ2014ZD40).

Notes and references

[a] CAS Key laboratory of Materials for Energy Conversion, Department of Materials Science and Engineering, University of Science and Technology of China, Hefei 230026, P. R. China.
[b] National Laboratory for Physical Sciences at the Microscale, University of Science and Technology of China, Hefei 230026, P. R. China.
[c] Synergetic Innovation Center of Quantum Information & Quantum Physics, University of Science and Technology of China, Hefei 230026, P. R. China. E-mail: fuzp@ustc.edu.cn, yllu@ustc.edu.cn

† Footnotes should appear here. These might include comments relevant to but not central to the matter under discussion, limited experimental and spectral data, and crystallographic data.

Electronic Supplementary Information (ESI) available: [Details on the characterization of different nanosheets array are included in the supplementary information]. See DOI: 10.1039/b000000x/

1 X. J. Feng, K. Shankar, O. K. Varghese, M. Paulose, T. J. Latempa and C. A. Grimes, *Nano Lett*, 2008, **8**, 3781.
2 A. Fujishima and K. Honda, *Nature*, 1972, **238**, 37.
3 D. H. Wang, D. W. Choi, J. Li, Z. G. Yang, Z. M. Nie, R. Kou, D. H. Hu, C. M. Wang, L. V. Saraf, J. G. Zhang, I. A. Aksay and J. Liu, *Acs Nano*, 2009, **3**, 907.
4 Q. Zheng, B. X. Zhou, J. Bai, L. H. Li, Z. J. Jin, J. L. Zhang, J. H. Li, Y. B. Liu, W. M. Cai and X. Y. Zhu, *Adv Mater*, 2008, **20**, 1044.
5 H. G. Yang, C. H. Sun, S. Z. Qiao, J. Zou, G. Liu, S. C. Smith, H. M. Cheng and G. Q. Lu, *Nature*, 2008, **453**, 638.
6 G. K. Mor, K. Shankar, M. Paulose, O. K. Varghese and C. A. Grimes, *Nano Lett*, 2006, **6**, 215.
7 S. J. Ding, J. S. Chen, Z. Y. Wang, Y. L. Cheah, S. Madhavi, X. A. Hu and X. W. Lou, *J Mater Chem*, 2011, **21**, 1677.
8 W. Q. Fang, J. Z. Zhou, J. Liu, Z. G. Chen, C. Yang, C. H. Sun, G. R. Qian, J. Zou, S. Z. Qiao and H. G. Yang, *Chem-Eur J*, 2011, **17**, 1423.
9 H. G. Yang, G. Liu, S. Z. Qiao, C. H. Sun, Y. G. Jin, S. C. Smith, J. Zou, H. M. Cheng and G. Q. Lu, *J Am Chem Soc*, 2009, **131**, 4078.
10 W. G. Yang, J. M. Li, Y. L. Wang, F. Zhu, W. M. Shi, F. R. Wan and D. S. Xu, *Chem Commun*, 2011, **47**, 1809.
11 F. Li, X. N. Li, R. R. Peng, X. F. Zhai, S. F. Yang, Z. P. Fu and Y. L. Lu, *Nanoscale*, 2014, **6**, 12434.
12 M. Cargnello, T. R. Gordon and C. B. Murray, *Chemical reviews*, 2014, **114**, 9319.
13 C. Dinh, T. Nguyen, F. Kleitz and T. Do, *Acs Nano*, 2009, **3**, 3737.
14 T. R. Gordon, M. Cargnello, T. Paik, F. Mangolini, R. T. Weber, P. Fornasiero and C. B. Murray, *J Am Chem Soc*, 2012, **134**, 6751.
15 B. B. Ni, F. Li, X. N. Li, Z. P. Fu, Y. W. Zhu and Y. L. Lu, *Appl Surf Sci*, 2013, **283**, 175.
16 J. Heinze, *Angew Chem Int Edit*, 1984, **23**, 831.
17 H. Xu, P. Reunchan, S. X. Ouyang, H. Tong, N. Umezawa, T. Kako and J. H. Ye, *Chem Mater*, 2013, **25**, 405.
18 H. Ariga, T. Taniike, H. Morikawa, M. Tada, B. K. Min, K. Watanabe, Y. Matsumoto, S. Ikeda, K. Saiki and Y. Iwasawa, *J Am Chem Soc*, 2009, **131**, 14670.

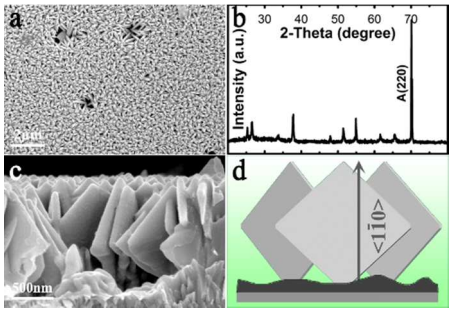

Upright diamond structured anatase nanosheets array with highly preferred orientation was obtained, which exhibited improved reduction capacity and electrochemical reversibility.